Submitted to ApJ 4 January 2008

Subtle Signatures of Multiplicity in Late-type Dwarf Spectra: The Unresolved M8.5/T5 Binary 2MASS J03202839−0446358

Adam J. Burgasser[1]

Massachusetts Institute of Technology, Kavli Institute for Astrophysics and Space Research, Building 37, Room 664B, 77 Massachusetts Avenue, Cambridge, MA 02139, USA; ajb@mit.edu

ABSTRACT

Evidence is presented that 2MASS J03202839−0446358, a nearby, peculiar, late-type dwarf, is an as-yet unresolved stellar/brown dwarf binary with late-type M dwarf and T dwarf components. This conclusion is based on new low-resolution, near-infrared spectroscopy that reveals a subtle but distinctive absorption feature at 1.6 μm. Previously noted in the peculiar L dwarf SDSS J080531.84+481233.0, this feature is shown to arise from the combination of FeH absorption from an M8.5 primary and pseudo-continuum flux from a T5±1 secondary, as ascertained from binary spectral templates constructed from empirical data. The 1.6 μm feature is also notably present in the combined light spectrum of the known M8.5 + T6 binary system SCR 1845-6357. The binary hypothesis resolves the known discrepancy between the optical and near-infrared classifications of 2MASS J0320−0446 (M8.5 and L1, respectively), while empirical binary templates provide a far superior match to its overall near-infrared spectral energy distribution. 2MASS J0320−0446 is the second very low mass binary to be identified solely by its low-resolution, near-infrared spectrum, and indicates that a wide variety of stellar/substellar binaries could be identified and characterized in this manner without the inherent limitations associated with high resolution imaging or spectroscopy.

Subject headings: stars: binaries: general — stars: fundamental parameters — stars: individual (2MASS J03202839−0446358) — stars: low mass, brown dwarfs

---

[1]Visiting Astronomer at the Infrared Telescope Facility, which is operated by the University of Hawaii under Cooperative Agreement NCC 5-538 with the National Aeronautics and Space Administration, Office of Space Science, Planetary Astronomy Program.

1. Introduction

The optical and near-infrared spectral energy distributions of very low mass stars and brown dwarfs—late-type M, L and T dwarfs—are distinctly non-blackbody. Overlapping molecular bands and strong line emission produce a rich array of spectral diagnostics for classification and characterization of physical properties. Considerable effort is now being devoted toward decrypting the spectral fingerprints of late-type dwarfs to determine masses, ages, metallicities and other fundamental parameters (e.g., Gorlova et al. 2003; McGovern et al. 2004; Kirkpatrick 2005; Burgasser, Burrows & Kirkpatrick 2007; Allers et al. 2007; Leggett et al. 2007; Liu, Leggett, & Chiu 2007; Burgasser et al. 2008). In some cases, spectral peculiarities arise when an observed source is in fact an unresolved multiple system, with components of different masses, effective temperatures, and spectral properties. While several classes of stellar multiples can been recognized on the basis of their unusual spectral or photometric properties (e.g., U Geminorum stars, M dwarf + white dwarf systems, etc.), identifying such cases amongst late-type dwarfs is complicated by the influence of other physical effects, such as low surface gravities, subsolar metallicities or unusual condensate cloud properties (e.g., Cruz et al. 2003, 2007; Knapp et al. 2004; Chiu et al. 2006; Kirkpatrick et al. 2006; Folkes et al. 2007; Burgasser et al. 2008). Differentiating between these various effects is essential if we hope to unambiguously characterize the physical properties of the lowest luminosity stars and brown dwarfs.

Very low mass multiple systems are important in their own right, as they enable mass and occasionally radius measurements (e.g., Bouy et al. 2004; Zapatero Osorio et al. 2004; Stassun et al. 2006), provide constraints for star/brown dwarf formation scenarios (e.g., Close et al. 2003; Maxted & Jeffries 2005; Allen 2007; Luhman et al. 2007b) and facilitate detailed studies of atmospheric properties (e.g., McCaughrean et al. 2004; Burgasser et al. 2006b; Liu et al. 2006; Martín et al. 2006; McElwain & Burgasser 2006). Of the roughly 90 very low mass multiple systems currently known[1], the majority have been identified through high angular resolution imaging, using the *Hubble Space Telescope* (e.g., Martín, Brandner & Basri 1999; Reid et al. 2001b, 2006a; Bouy et al. 2003; Burgasser et al. 2003, 2006b; Gizis et al. 2003) and, increasingly, ground-based adaptive optics systems (e.g., Close et al. 2002, 2003, 2007; Potter et al. 2002; Siegler et al. 2003, 2005, 2007; Chauvin et al. 2004; McCaughrean et al. 2004; Kraus, White & Hillenbrand 2005; Liu & Leggett 2005; Gelino, Kulkarni & Stephens 2006; Liu et al. 2006; Phan-Bao et al. 2006; Looper et al. 2008). However, as the vast majority of very low mass binaries have small separations (>90% have $\rho < 20$ AU; Allen 2007), expanding the population of known binaries to greater distances requires either finer angular

[1]A current list is maintained by N. Siegler at http://www.vlmbinaries.org.

sampling or the identification of systems that are unresolved. In addition, the frequency of nearby, tightly-bound binaries is essential for a complete assessment of the overall very low mass dwarf binary fraction, since imaging studies provide only a lower limit to this fundamental statistic. Such systems are also more likely to eclipse, enabling badly-needed radius measurements (e.g., Stassun et al. 2006). While searches for radial velocity variability via high resolution spectroscopy are useful in this regime (e.g., Basri & Martín 1999; Reid et al. 2002; Guenther & Wuchterl 2003; Kenyon et al. 2003; Basri & Reiners 2006; Blake et al. 2007; Joergens & Müller 2007), in most cases very low luminosity or distant late-type dwarfs are too faint to be followed up in this manner.

Recently, Burgasser (2007c) has demonstrated that, in certain special cases, the presence of an unresolved companion can be inferred directly from the appearance of a source's low-resolution near-infrared spectrum. In particular, it was shown that the spectrum of the peculiar L dwarf SDSS J080531.84+481233.0 (hereafter SDSS J0805+4812; Hawley et al. 2002; Knapp et al. 2004), which has highly discrepant optical and near-infrared spectral classifications, could be accurately reproduced as a combination of "normal" L4.5 plus T5 components. Indeed, the binary hypothesis provides a far simpler and more consistent explanation for the unusual optical, near-infrared and mid-infrared properties of SDSS J0805+4812 than other alternatives (e.g., Knapp et al. 2004; Folkes et al. 2007; Leggett et al. 2007). The identification of other unresolved multiples like SDSS J0805+4812 by low-resolution near-infrared spectroscopy is a potential boon for low mass multiplicity studies, as this method is not subject to the physical or projected separation limitations inherent to high-resolution imaging and spectroscopic techniques, and is far less resource-intensive.

This article reports the second unresolved very low mass binary system, 2MASS J03202839−0446358 (hereafter 2MASS J0320−0446), to be identified on the basis of its low-resolution near-infrared spectrum. New observations leading to this conclusion are presented in § 2, along with near-infrared and optical classifications and evidence of subtle spectral features indicating the presence of a T dwarf secondary. Analysis of the near-infrared spectrum of 2MASS J0320−0446 using the binary template matching technique described in Burgasser (2007c) is presented in § 3. § 4 discusses the results of this analysis, provides further evidence of unresolved multiplicity by examination of the composite spectrum of the known M dwarf/T dwarf binary SCR 1845-6357, and explores limitations in the identification of such binaries via near-infrared spectroscopy. Conclusions are summarized in § 5.

2. Observations

2.1. Previous Observations of 2MASS J0320−0446

2MASS J0320−0446 was originally discovered by Cruz et al. (2003) and Wilson et al. (2003) in the Two Micron All Sky Survey (2MASS; Skrutskie et al. 2006), and classified M8: (uncertain) and L0.5 on the basis of optical and near-infrared spectroscopy, respectively. The M8 optical classification is uncertain due to the low signal-to-noise of the spectral data (see below). Cruz et al. (2003) estimate a distance of 26 pc for this source based on this classification and empirical M_J/spectral type relations. Deacon, Hambly & Cooke (2005), using I-band plate data from the SuperCosmos Sky Survey (SSS; Hambly et al. 2001a,b,c), determined a proper motion of $0\farcs68\pm0\farcs04$ yr^{-1} at position angle 191°, making 2MASS J0320−0446 a relatively high proper motion source. Figure 1 shows the field around 2MASS J0320−0446 imaged by R and I photographic plates and 2MASS (JHK_s). A faint source is seen in the 1955 Palomar Sky Survey I (Abell 1959) R-band image roughly at the offset position indicated by the Deacon, Hambly & Cooke (2005) proper motion. By including this source position along with additional astrometry drawn from the SSS and 2MASS catalogs (Table 1), an improved proper motion measurement of $0\farcs562\pm0\farcs005$ yr^{-1} at position angle 205.9 ± 0.5° was determined. This proper motion and the distance estimate above indicates a rather large tangential space velocity, $V_{tan} \approx 70$ km s^{-1}, suggesting that 2MASS J0320−0446 could be an older disk star. None of these previous studies report the presence of a faint companion to this source.

2.2. Near-Infrared Spectroscopy

Low resolution near-infrared spectral data for 2MASS J0320−0446 were obtained on 2007 September 16 (UT) using the SpeX spectrograph (Rayner et al. 2003) mounted on the 3m NASA Infrared Telescope Facility (IRTF). The conditions on this night were poor with patchy clouds, cirrus and average seeing ($0\farcs8$ at J-band), and 2MASS J0320−0446 was observed as a bright backup target ($J = 12.13\pm0.03$). The $0\farcs5$ slit was used to obtain 0.7–2.5 μm spectroscopy with resolution $\lambda/\Delta\lambda \approx 120$ and dispersion across the chip of 20–30 Å pixel^{-1}. To mitigate the effects of differential refraction, the slit was aligned to the parallactic angle. Six exposures of 90 s each were obtained in an ABBA dither pattern along the slit. The A0 V star HD 18571 was observed immediately after 2MASS J0320−0446 and at a similar airmass (1.21) for flux calibration. Internal flat field and argon arc lamps were observed after both target and flux standard observations for pixel response and wavelength calibration. Data were reduced with the IDL SpeXtool package, version 3.4 (Cushing, Vacca,

& Rayner 2004; Vacca et al. 2003), using standard settings. A detailed description of the reduction procedures are given in Burgasser (2007c).

The near-infrared spectrum of 2MASS J0320−0446 is shown in Figure 2, compared to equivalent data for the optical spectral standards VB 10 (M8; van Biesbroeck 1961; Kirkpatrick, Henry, & McCarthy 1991) and 2MASS J14392836+1929149 (L1, hereafter 2MASS J1439+1929; Kirkpatrick et al. 1999). Despite the poor observing conditions, the data for 2MASS J0320−0446 have exceptionally good signal-to-noise, $\gtrsim$150 in the JHK flux peaks and $\sim$50 in the bottom of the 1.4 and 1.8 μm H_2O bands. Color biases due to telluric cloud absorption are also apparently absent, as indicated by the agreement between synthetic $J-H$, $H-K_s$ and $J-K_s$ colors to 2MASS measurements to within the photometric uncertainties of the latter. The morphology of the near-infrared spectrum of 2MASS J0320−0446 is overall very similar to that of a typical late-type M or early-type L dwarf, with bands of TiO and VO absorption at red optical wavelengths ($\lambda < 1$ μm); prominent H_2O absorption at 1.4 and 1.8 μm; FeH absorption at 0.99, 1.2 and 1.55 μm; Na I and K I line absorption in the 1.0-1.3 μm region; weak Na I lines at 2.2 μm; and strong CO bandheads at 2.3–2.4 μm. For the most part, the spectrum of 2MASS J0320−0446 is more consistent with that of 2MASS J1439+1929; note in particular the similarities in the overall shape of the 1.0–1.35 μm J-band flux peak and the deep 1.4 μm H_2O band. However, TiO and VO bands are more similar to (but weaker than) those seen in the spectrum of VB 10, while the weak 2.2 μm Na I lines are rarely seen in L dwarf spectra (e.g., McLean et al. 2003). The near-infrared spectrum of 2MASS J0320−0446 is also somewhat bluer than that of 2MASS J1439+1929, in line with their respective colors ($J-K_s = 1.13\pm0.04$ versus 1.21 ± 0.03).

2MASS J0320−0446 exhibits one unusual feature not seen in either comparison spectrum, namely a slight dip at 1.6 μm indicated by an asterisk in Figure 2. This subtle but remarkable feature is discussed further below.

2.3. Classification of 2MASS J0320−0446

The overall similarity of the SpeX spectrum of 2MASS J0320−0446 to that of 2MASS J1439+1929 indicates an L1 near-infrared spectral type for this source. This is confirmed by examination of the spectral indices (Table 2) and index/spectral type relations defined by Reid et al. (2001a) and Geballe et al. (2002). The average subtype for the four indices K1 (measuring the shape of the K-band flux peak), H_2O-A, H_2O-B and H_2O-1.5 (all measuring the strength of the 1.4 μm H_2O band) yields a near-infrared classification of L1 ($\pm$0.6 subtypes), consistent with the L0.5 near-infrared classification reported by Wilson et al. (2003).

This near-infrared spectral type is fully three subtypes later than the M8: optical spectral type reported by Cruz et al. (2003). To verify this discrepancy, optical data from the Cruz et al. study were compared directly against those for the optical spectral standards 2MASS J14342644+1940499 (M8; hereafter 2MASS J1434+1904) LHS 2065 (M9), 2MASS J03454316+2540233 (L0; hereafter 2MASS J0345+2540) and 2MASS J1439+1929 (Kirkpatrick, Henry, & McCarthy 1991; Kirkpatrick et al. 1999), as illustrated in Figure 3. The optical spectrum of 2MASS J0320−0446 does not perfectly match any of the comparison spectra, but shows good agreement with LHS 2065 shortward of 7300 Å and with 2MASS J1434+1904 in the 7700–8300 Å range; note in particular the similar strengths of the Na I doublet at 8183/8195 Å. 2MASS J0320−0446 does not appear to have an L dwarf optical spectrum, given the strength of the Na I lines and TiO bands at 7200 Å and 8500 Å. This is confirmed again by the spectral indices (Table 2) and spectral index relationships from Martín et al. (1999); Geballe et al. (2002); and Lépine, Rich, & Shara (2003a). The VO2 (measuring the strength of the 7900 Å VO band), TiO7 (measuring the strength of the 8400 Å TiO band) and PC3 index (measuring spectral color) yield a mean optical subtype of M8.5 (±0.6 subtypes). This is consistent with the uncertain classification reported by Cruz et al. (2003) and 2.5 subtypes earlier than the near-infrared classification.

A discrepancy between near-infrared and optical spectral types is not altogether uncommon amongst late-type dwarfs. Geballe et al. (2002) found disagreements of up to 1.5 subtypes between optical (based on the Kirkpatrick et al. 1999 scheme) and near-infrared classifications (based on their own scheme) of several L dwarfs. Knapp et al. (2004) identified sources whose optical spectral types were at least one subtype earlier than their near-infrared spectral types. Burgasser et al. (2008) have discussed in detail a subclass of blue L dwarfs whose optical classifications are consistently 2-3 subtypes earlier than their near-infrared classifications. Such discrepancies have been variously attributed to surface gravity, metallicity, condensate cloud or multiplicity effects (e.g., Gizis et al. 2000; Cruz et al. 2003, 2007; McLean et al. 2003; Knapp et al. 2004; Burgasser et al. 2005, 2008; Chiu et al. 2006; Burgasser, Cruz & Kirkpatrick 2007; Folkes et al. 2007). Surface gravity effects are certainly possible in this case, as the large V_{tan} of 2MASS J0320−0446 suggests that it may be a relatively old system. For the same reason, slightly subsolar metallicities and thin condensate clouds (whose effects are less pronounced in late-type M dwarfs) may also be relevant.

However, it is the weak absorption feature at 1.6 μm in the spectrum of 2MASS J0320−0446 that suggests multiplicity as being the cause for the discrepant classifications. This feature is nearly coincident with the 1.57-1.64 μm FeH absorption band commonly observed in L dwarf near-infrared spectra (Wallace & Hinkle 2001; Cushing et al. 2003). Yet its morphology is clearly different, with a cup-shaped depression as opposed to the flat plateau seen in the comparison spectra of Figure 2. More importantly, this feature has the same morphol-

ogy and is centered at the same wavelength as the peculiar feature noted in the spectrum of SDSS J0805+4812 (Burgasser 2007c). In that case, the 1.6 μm feature was found to arise from the contribution of light from a mid-type T dwarf companion. Given the similar discrepancy in optical and near-infrared classifications and the presence of this unusual feature in the spectra of both SDSS J0805+4812 and 2MASS J0320−0446, it is reasonable to consider whether the latter also harbors a faint T dwarf companion.

3. Binary Template Matching

3.1. Spectral Sample

To test this hypothesis, a variant of the binary spectral template matching technique described in Burgasser (2007c) was employed.[2] In this method, the spectrum of a late-type source is compared to a large set of binary spectra constructed from an empirical sample of M, L and T dwarf spectra. To minimize systematic effects, the source and template spectra should have the same spectral resolution and coverage. This requirement was facilitated through the use of a large sample of nearly 200 SpeX prism spectra of M5–T8 dwarfs drawn from the literature[3] or from the author's unpublished observations. Spectral types for the sources in this sample were assigned according to published classifications[4], based either on the optical classification schemes of Kirkpatrick, Henry, & McCarthy (1991) and Kirkpatrick et al. (1999) for M5–L8 dwarfs or the near-infrared classification scheme of Burgasser et al. (2006a) for L9–T8 dwarfs (M and L dwarfs with only near-infrared classifications reported were rejected). The initial spectral sample was purged of low signal-to-noise data as well as spectra of those sources known to be binary or noted as peculiar in the literature (e.g., low surface gravity brown dwarfs, subdwarfs and blue L dwarfs). This left a sample of 133 spectra of 126 sources, listed in Table 3. The distribution of spectral types in this sample is illustrated in Figure 4. There is a paucity of L5–L9 dwarfs, but this does not adversely impact the analysis.

---

[2]See also Burgasser et al. (2005, 2006b, 2008); Reid et al. (2006b); Burgasser (2007b); Looper, Kirkpatrick & Burgasser (2007); and Siegler et al. (2007).

[3]See Burgasser et al. (2004, 2006a); Cruz et al. (2004); Burgasser, Burrows & Kirkpatrick (2007); Burgasser & McElwain (2006); Chiu et al. (2006); McElwain & Burgasser (2006); Reid et al. (2006b); Burgasser (2007a,b); Burgasser et al. (2007a); Liebert & Burgasser (2007); Looper, Kirkpatrick & Burgasser (2007); and Luhman et al. (2007b).

[4]A current list of L and T dwarfs with their published optical and near-infrared spectral types is maintained by C. Gelino, J. D. Kirkpatrick and A. Burgasser at http://www.dwarfarchives.org.

3.2. Single Template Fits

In order to ascertain whether an unresolved binary truly provides a better fit to the spectrum of 2MASS J0320−0446, comparisons were first made to the individual sources in the SpeX sample. All spectra were initially normalized to their peak flux in the 1.2–1.3 μm band. Chi-square deviations[5] (χ^2) were then computed between the spectrum of 2MASS J0320−0446 and each template spectrum over the 0.95–1.35 μm, 1.45–1.8 μm and 2.0–2.35 μm regions. To eliminate normalization bias, each template spectrum was additionally scaled by a multiplicative factor in the range 0.5–1.5 to minimize χ^2.

Figure 5 displays the four best single template matches, all having $\chi^2 < 0.6$. The three best-fitting sources—LEHPM 1-6333 (M8), 2MASS J1124+3808 (M8.5) and LEHPM 1-6443 (M8.5)—have optical spectral types consistent with the optical type of 2MASS J0320−0446. Furthermore, the LEHPM[6] sources have relatively large proper motions ($\mu > 0\farcs4$ yr^{-1}), similar to 2MASS J0320−0446. All four sources shown in Figure 5 provide reasonably good matches to the broad near-infrared spectral energy distribution of 2MASS J0320−0446, but with two key discrepancies: an absence of the 1.6 μm feature (inset boxes in Figure 5) and a shortfall in the peak spectral flux at 1.27 μm. In the former case, FeH absorption bands are clearly seen in the spectra of the M dwarf/L dwarf comparison spectra, but do not produce the sharp dip seen in the spectrum of 2MASS J0320−0446. In the latter case, the spectrum of 2MASS J0320−0446 is consistently brighter in the 1.2–1.35 μm range as compared to the M dwarf templates. As demonstrated below, both of these discrepancies can be resolved by the addition of a T dwarf component.

3.3. Binary Template Fits

Binary spectral templates from the SpeX prism sample were constructed by first flux-calibrating each spectrum according to established absolute magnitude/spectral type relations. For M5-L5 dwarfs, the 2MASS M_J relation of Cruz et al. (2003) was used. For L5-T8 dwarfs, both of the two MKO[7] M_K/spectral type relations defined in Liu et al. (2006) were considered. The Liu et al. relations are based on a sample of L and T dwarfs with measured

[5]Here, $\chi^2 \equiv \sum_{\{\lambda\}} \frac{[f_\lambda(0320)-f_\lambda(T)]^2}{f_\lambda(0320)}$, where $f_\lambda(0320)$ is the spectrum of 2MASS J0320−0446 and $f_\lambda(T)$ the template spectrum, and the sum is performed over the set of wavelengths $\{\lambda\}$ as specified in the text.

[6]Liverpool-Edinburgh High Proper Motion (LEHPM) Catalog of Pokorny et al. (2004).

[7]Mauna Kea Observatory (MKO) photometric system; Simons & Tokunaga (2002); Tokunaga, Simons & Vacca (2002).

pallaxes and MKO photometry, but one relation ("bright") was constructed after rejecting known (resolved) binaries while the other relation ("faint") was constructed after rejecting all known and candidate binaries as justified in that study. As illustrated in Figure 3 of Burgasser (2007b), these two relations envelope the M_K values of currently measured sources (including components of resolved binaries), but diverge by as much as ∼1 mag for spectral types L8–T5. Nevertheless, these relations represent our current best constraints on the absolute magnitude/spectral type relation across the L dwarf/T dwarf transition. In all cases, synthetic magnitudes to scale the data were calculated directly from the spectra. Binary templates were then constructed by adding together the calibrated spectra of source pairs whose types differ by at least 0.5 subclasses, producing a total of 8511 unique combinations. The binary templates were then normalized to their peak flux in the 1.2–1.3 μm band and compared to the spectrum of 2MASS J0320−0446 in the same manner as the single source templates; i.e., with additional scaling to minimize χ^2.

Figure 6 displays the best fitting binary templates constructed from the primaries shown in Figure 5 and using the "faint" M_K/spectral type relation of Liu et al. (2006). For all four cases, the addition of a mid-type T dwarf secondary spectrum considerably improves the spectral template match. In particular, the 1.6 μm spectral dip is very well reproduced in all cases, while the flux peaks at 1.27 μm in the binary templates are more consistent with the spectrum of 2MASS J0320−0446. Even detailed alkali line and FeH features in the 0.9–1.3 μm region are better matched with the binary templates.

Figure 7 displays the best fitting binary templates using the "bright" M_K/spectral type relation of Liu et al. (2006). There is a small degree of improvement in these fits over those using the "faint" M_K relation, although the differences are very subtle due to the very small contribution of light by the T dwarf secondaries ($\Delta J \approx 3.5$ mag, depending on the components). This result is fortuitous, as it indicates that the better fits provided by the binary templates are only weakly dependent on the absolute magnitude relation assumed over a spectral type range in which such relations are currently most uncertain.

Besides the best-fit comparisons shown in Figures 6 and 7, there were many excellent matches ($\chi^2 < 0.1$) found among binaries templates which had LEHPM 1-6333 or 2MASS J1124+3808 as primaries: 30 for the "faint" M_K/spectral type relation and 58 for the "bright" relation. The average primary and secondary spectral types for the combinations in this well-matched sample are M8.5±0.3 and T5.0±0.9, respectively, with no significant differences between analyses using the "faint" or "bright" M_K/spectral type relations. The mean relative magnitudes of the primary and secondary components are $\Delta J = 3.1\pm0.4$ mag, $\Delta H = 3.8\pm0.5$ mag, $\Delta K = 4.3\pm0.6$ mag for the "bright" relation and $\Delta J = 3.5\pm0.2$ mag, $\Delta H = 4.3\pm0.3$ mag, $\Delta K = 4.9\pm0.3$ mag for the "faint" relation, as calculated directly

from the flux-calibrated spectral templates. Hence, there is a significant difference in the relative magnitudes between the components between these two relations, indicating a potential means of distinguishing which more accurately describes the absolute magnitudes of mid-type T dwarfs.

The origin of the 1.6 μm feature in the spectrum of 2MASS J0320−0446 is clearly revealed in Figures 6 and 7: it is a combination of FeH absorption in the M dwarf primary and CH_4 absorption in the T dwarf secondary. Specifically, the relatively sharp H-band flux peak in the spectrum of the T dwarf secondary blueward of the 1.6 μm CH_4 band contributes light to the 1.55–1.6 μm spectrum of the composite system. This is on the blue end of the 1.55-1.65 μm FeH absorption band, producing a distinct "dip" feature. Similarly, the apparently brighter 1.2–1.35 μm flux in the spectrum of 2MASS J0320−0446 can be attributed to the T dwarf companion, which exhibits a narrow J-band peak between strong 1.1 μm and 1.4 μm H_2O and CH_4 bands. Both features are therefore unique to binaries containing late-type M and L dwarf primaries (in which FeH is prominent) and T dwarf secondaries.

4. Discussion

4.1. Is 2MASS J0320−0446 an M dwarf/T dwarf Binary?

It may be concluded from the analysis above that the near-infrared spectrum of 2MASS J0320−0446, including the subtle feature observed at 1.6 μm, can be accurately reproduced by assuming that this source is an unresolved M8.5 + T5 binary. But does this mean that 2MASS J0320−0446 actually is a binary? This could be proven by high-resolution imaging observations, although if the system is not resolved it would not rule out the presence of a closely-separated binary companion (separations $\lesssim 0\farcs25 \approx 6$ AU would be marginally resolvable with *HST* for this system's component magnitudes; Burgasser et al. 2006b). High resolution spectroscopic monitoring could potentially reveal radial velocity signatures in the former case, although this depends on the separation and mass of the system components.

An alternative test of the binary hypothesis for 2MASS J0320−0446 is to identify similar spectral traits in a comparable binary system. Fortunately, one such system is known: the M8.5 + T6 binary SCR 1845-6357 (Hambly et al. 2004; Biller et al. 2006). This nearby (3.85±0.02 pc; Henry et al. 2006), well-resolved binary ($\rho = 1\farcs1$) has individually classified components based on resolved spectroscopy (Kasper et al. 2007). More importantly, the relative near-infrared magnitudes of this system ($\Delta J = 3.68\pm0.03$ mag, $\Delta H = 4.20\pm0.04$ mag, $\Delta K = 5.12\pm0.03$ mag Kasper et al. 2007) are somewhat larger than but consistent with the

estimated relative magnitudes of the putative 2MASS J0320−0446 system. Figure 8 displays the component spectra of this system, scaled to their relative H-band magnitudes[8], as well as the sum of the component spectra. The composite spectrum shows a relative increase in spectral flux as compared to the primary in both the 1.2–1.35 μm and 1.55–1.6 μm regions. Indeed, the latter gives rise to the same "dip" feature observed in the H-band spectrum of 2MASS J0320−0446, particularly when the SCR 1845-6357AB data are reduced in resolution to match that of the SpeX prism data (inset box in Figure 8). The presence of this feature in the composite spectrum of a known M dwarf/T dwarf binary lends considerable confidence to the conclusion that 2MASS J0320−0446 is itself an M dwarf/T dwarf binary.

Assuming then that 2MASS J0320−0446 is an M8.5 + T5 dwarf binary, it is possible to characterize the components in some detail based on the analysis in § 3.3. Synthetic component JHK magnitudes on the MKO system assuming the "bright" M_K/spectral type relation were computed from the best-fitting binary templates ($\chi^2 < 0.1$) and are listed in Table 4. The M dwarf primary is only slightly fainter than the composite source, while the T dwarf companion is exceptionally faint, $J = 16.4\pm0.4$ mag. This is consistent with the estimated distance of the primary, 25±3 pc, based on the M_J/spectral type relation of Cruz et al. (2003). The estimated photometry of the secondary is close to the detection limits of 2MASS, and explains why this component, even if widely separated from its primary, has not been detected in survey images. The low luminosity of the secondary, $\log_{10} L_{bol}/L_{\odot}$ = -5.0±0.3 dex based on its inferred spectral type (Golimowski et al. 2004; Burgasser 2007b), suggests that 2MASS J0320−0446 could have a relatively low system mass ratio (M_2/M_1). This depends on its age of the system, for which there are no robust constraints. Using the evolutionary models of Burrows et al. (1997) and component luminosities as listed in Table 4, primary and secondary mass estimates for ages of 1, 5 and 10 Gyr were derived. If 2MASS J0320−0446 is an older system, as suggested by its large V_{tan}, its inferred mass ratio $M_2/M_1 > 0.8$ would be consistent with the typical mass ratios of very low mass binaries in the field (Burgasser et al. 2007b).

---

[8]The J-band portion of the spectrum of SCR 1845-6357A shown here is slightly reduced relative to the H- and K_s-band spectra as compared to Figure 2 in Kasper et al. (2007). The relative flux calibration between spectral orders applied in that study did not account for missing data over 1.33–1.50 μm, slightly inflating the flux levels in the J-band. A recalibration of this spectrum was made by scaling each order by a constant factor to match the SpeX prism spectrum of 2MASS J1124+3808, which has a similar $J - K_s$ color (1.14±0.03 versus 1.06±0.03 for SCR 1845-6357 from Kasper et al. 2007) and optical spectral type (M8.5). Such recalibration is not necessary for the SCR 1845-6357B spectrum due to the strong 1.35 μm CH_4 and 1.4 μm H_2O bands in this source. The recalibration of the SCR 1845-6357A J-band spectrum does not affect the analysis presented here, which depends solely on the relative H-band scaling of the component spectra.

4.2. Recognizing M dwarf/T dwarf Binaries from Composite Near-Infrared Spectra

The subtlety of the peculiar features present in the composite spectra of 2MASS J0320−0446 and SCR 1845-6357 are due entirely to the very small flux ratios between their M and T dwarf components, a factor of less than 1/100 in the K-band in the case of SCR 1845-6357. Yet in both cases the 1.6 μm feature, indicating the presence of a T dwarf companion, can be discerned. If other equivalent systems are to be found, it is pertinent to assess the earliest-type primary for which a T dwarf companion can be identified in this manner, and the variety of T dwarf companions that could be discerned. Figure 9 displays binary spectral templates for four primary types—M7, M8, M9 and L0—combined with T0–T8 dwarf secondaries. For all three cases, the 1.6 μm feature is most pronounced when the secondary is a mid-type T dwarf, spectral types T3–T5. This is due to a tradeoff in the sharpness of the H-band flux peak in this component (i.e., the strength of its 1.6 μm CH_4 absorption) and its brightness relative to the primary. Not surprisingly, the 1.6 μm feature is more pronounced in binaries with later-type primaries, making it a useful multiplicity diagnostic for systems with L dwarf primaries (such as SDSS J0805+4812), but far more subtle in systems with M dwarf primaries. Indeed, the spectra in Figure 9 suggest that this feature is basically undetectable in binaries with M7 and earlier-type primaries. 2MASS J0320−0446 and SCR 1845-6357 probably contain the earliest-type primaries for which a T dwarf secondary could be identified solely from their composite near-infrared spectra.

It is important to also reflect on the other key spectral peculiarity caused by the presence of a T dwarf companion, the slight increase in flux at 1.3 μm. This feature increases the contrast in the 1.4 μm H_2O band, and therefore serves to bias H_2O spectral indices toward later subtypes. This effect explains why the near-infrared classification of 2MASS J0320−0446 is so much later than its optical classification (the T dwarf secondary contributes negligibly in the optical). Figure 9 shows that the 1.3 μm flux increase can be discerned for systems with early- and mid-type T dwarf companions, and while it is again more pronounced for the later-type binaries it is still present (but subtle) in the spectra of systems with M7 primaries. Unusually strong absorption at 1.35 μm can therefore be an indicator of the presence of a T dwarf companion. However, other effects, notably reduced condensate opacity (Burgasser et al. 2008), also gives rise to this same spectral peculiarity. Hence, both the contrast of the 1.4 μm H_2O band and the presence of the 1.6 μm dip should be considered together as indicators of an unresolved T dwarf companion.

A more practical limitation in identifying M dwarf/T dwarf binaries based on their composite near-infrared spectra is the availability of uniformly flux calibrated data for a large sample of non-peculiar spectral template sources. This issue is resolved here through

the use of a large, screened dataset of well-calibrated, high signal-to-noise SpeX prism data, which the author has made available online.[9] However, even in this sample unresolved binaries or otherwise peculiar sources may exist, and the definition of "peculiar" will depend on what kind of system is being studied (e.g., young binaries will have components with low surface gravity features). Building up spectral samples such as the SpeX prism dataset used here is an important step toward uncovering additional examples of unresolved M dwarf/L dwarf + T dwarf binaries.

5. Conclusions

This article has attempted to demonstrate that subtle peculiarities observed in the near-infrared spectrum of 2MASS J0320−0446, in particular a characteristic bowl-shaped dip at 1.6 μm, indicate the presence of an as-yet unresolved mid-type T dwarf companion. This scenario not only provides a simple and straightforward explanation for the 1.6 μm feature—also present in the composite spectrum of the known M8.5 + T6 binary SCR 1845-6357—but also resolves the discrepancy between the optical and near-infrared classifications of 2MASS J0320−0446. Furthermore, empirical binary templates composed of "normal" M dwarf plus T dwarf pairs provide a far superior match to the overall near-infrared spectral energy distribution of 2MASS J0320−0446 than any single comparison source. The hypothesis that 2MASS J0320−0446 is an unresolved binary is therefore compelling, and could potentially be verified through high resolution imaging and/or radial velocity monitoring observations.

The author would like to thank telescope operator Paul Sears and instrument specialist John Rayner at IRTF for their assistance during the observations; Markus Kasper for providing the spectral data for SCR 1845-6357; Kelle Cruz for providing optical spectral data for 2MASS J0320−0446; and Kelle Cruz, Sandy Leggett, Dagny Looper and Kevin Luhman for providing a portion of the SpeX prism spectra used in the binary spectral template analysis. This publication makes use of data from the Two Micron All Sky Survey, which is a joint project of the University of Massachusetts and the Infrared Processing and Analysis Center, and funded by the National Aeronautics and Space Administration and the National Science Foundation. 2MASS data were obtained from the NASA/IPAC Infrared Science Archive, which is operated by the Jet Propulsion Laboratory, California Institute of Technology, under contract with the National Aeronautics and Space Administration. This research has

[9]See http://www.browndwarfs.org/spexprism.

benefitted from the M, L, and T dwarf compendium housed at DwarfArchives.org and maintained by Chris Gelino, Davy Kirkpatrick, and Adam Burgasser; and the VLM Binaries Archive maintained by Nick Siegler at http://www.vlmbinaries.org. The authors wish to recognize and acknowledge the very significant cultural role and reverence that the summit of Mauna Kea has always had within the indigenous Hawaiian community. We are most fortunate to have the opportunity to conduct observations from this mountain.

Facilities: IRTF (SpeX)

REFERENCES

Abell, G. O. 1959, PASP, 67, 258

Allen, P. R. 2007, ApJ, 668, 492

Allers, K. N., et al. 2007, ApJ, 657, 511

Artigau, É, Doyon, R., Lafrenière, D., Nadeau, D., Robert, J., & Albert, L. 2006, ApJ, 651, L57

Basri, G., & Reiners, A. 2006, AJ, 132, 663

Basri, G., & Martín, E. L. 1999, AJ, 118, 2460

Biller, B. A., Kasper, M., Close, L. M., Brandner, W., & Kellner, S. 2006, ApJ, 641, L141

Blake, C. H., Charbonneau, D., White, R. J., Marley, M. S., & Saumon, D. 2007, ApJ, 666, 1198

Bouy, H., Brandner, W., Martín, E. L., Delfosse, X., Allard, F., Baraffe, I., Forveille, T., & Demarco, R. 2004, A&A, 424, 213

Bouy, H., Brandner, W., Martín, E. L., Delfosse, X., Allard, F., & Basri, G. 2003, AJ, 126, 1526

Burgasser, A. J. 2007a, ApJ, 658, 617

Burgasser, A. J. 2007b, ApJ, 659, 655

Burgasser, A. J. 2007c, AJ, 134, 1330

Burgasser, A. J., Burrows, A. & Kirkpatrick, J. D. 2006, ApJ, 639, 1095

Burgasser, A. J., Cruz, K. L., & Kirkpatrick, J. D. 2007, ApJ, 657, 494

Burgasser, A. J., Geballe, T. R., Leggett, S. K., Kirkpatrick, J. D., & Golimowski, D. A. 2006a, ApJ, 637, 1067

Burgasser, A. J., & Kirkpatrick, J. D. 2008, AJ, in preparation

Burgasser, A. J., Kirkpatrick, J. D., Cruz, K. L., Reid, I. N., Leggett, S. K., Liebert, Burrows, A., & Brown, M. E. 2006b, ApJS, 166, 585

Burgasser, A. J., Kirkpatrick, J. D., Liebert, J., & Burrows, A. 2003a, ApJ, 594, 510

Burgasser, A. J., Kirkpatrick, J. D., McElwain, M. W., Cutri, R. M., Burgasser, A. J., & Skrutskie, M. F. 2003b, AJ, 125, 850

Burgasser, A. J., Kirkpatrick, J. D., Reid, I. N., Brown, M. E., Miskey, C. L., & Gizis, J. E. 2003, ApJ, 586, 512

Burgasser, A. J., Looper, D. L., Kirkpatrick, J. D., & Swift, B. 2008, ApJ, in press

Burgasser, A. J., Looper, D. L., Kirkpatrick, J. D., & Liu, M. C. 2007a, ApJ, 658. 557

Burgasser, A. J., & McElwain, M. W. 2006, AJ, 131, 1007

Burgasser, A. J., McElwain, M. W., & Kirkpatrick, J. D. 2003, AJ, 126, 2487

Burgasser, A. J., McElwain, M. W., Kirkpatrick, J. D., Cruz, K. L., Tinney, C. G., & Reid, I. N. 2004b, AJ, 127, 2856

Burgasser, A. J., Reid, I. N., Leggett, S. J., Kirkpatrick, J. D., Liebert, J., & Burrows, A. 2005, ApJ, 634, L177

Burgasser, A. J., Reid, I. N., Siegler, N., Close, L. M., Allen, P., Lowrance, P. J., & Gizis, J. E. 2007b, in Planets and Protostars V, eds. B. Reipurth, D. Jewitt and K. Keil (Univ. Arizona Press: Tucson), p. 427

Burgasser, A. J., et al. 1999, ApJ, 522, L65

Burgasser, A. J., et al. 2000a, ApJ, 531, L57

Burgasser, A. J., et al. 2000b, AJ, 120, 1100

Burgasser, A. J., et al. 2002, ApJ, 564, 421

Burrows, A., et al. 1997, ApJ, 491, 856

Chauvin, G., Lagrange, A.-M., Dumas, C., Zuckerman, B., Mouillet, D., Song, I., Beuzit, J.-L., & Lowrance, P. 2004, A&A, 425, L29

Chiu, K., Fan, X., Leggett, S. K., Golimowski, D. A., Zheng, W., Geballe, T. R., Schneider, D. P., & Brinkmann, J. 2006, AJ, 131, 2722

Close, L. M., Siegler, N., Freed, M., & Biller, B. 2003, ApJ, 587, 407

Close, L. M., Siegler, N., Potter, D., Brandner, W., & Liebert, J. 2002, ApJ, 567, L53

Close, L. M., et al. 2007, ApJ, 660, 1492

Cruz, K. L., Burgasser, A. J., Reid, I. N., & Liebert, J. ApJ, 2004, 604, L61

Cruz, K. L., Reid, I. N., Liebert, J., Kirkpatrick, J. D., & Lowrance, P. J. 2003, AJ, 126, 2421

Cruz, K. L., et al. 2007, AJ, 133, 439

Cushing, M. C., Rayner, J. T., Davis, S. P., & Vacca, W. D. 2003, ApJ, 582, 1066

Cushing, M. C., Vacca, W. D., & Rayner, J. T. 2004, PASP, 116, 362

Deacon, N. R., Hambly, N. C., & Cooke, J. A. 2005, A&A, 435, 363

Ellis, S. C., Tinney, C. G., Burgasser, A. J., Kirkpatrick, J. D., & McElwain, M. W. 2005, AJ, 130, 2347

Folkes, S. L., Pinfield, D. J., Kendall, T. R., & Jones, H. R. A. 2007, MNRAS, 378, 901

Geballe, T. R., et al. 2002, ApJ, 564, 466

Gelino, C. R., Kulkarni, S. R., & Stephens, D. C. 2006, PASP, 118, 611

Gizis, J. E. 2002, ApJ, 575, 484

Gizis, J. E., Kirkpatrick, J. D., & Wilson, J. C. 2001, AJ, 121, 2185

Gizis, J. E., Monet, D. G., Reid, I. N., Kirkpatrick, J. D., Liebert, J., & Williams, R. 2000, AJ, 120, 1085

Gizis, J. E., Reid, I. N., Knapp, G. R., Liebert, J., Kirkpatrick, J. D., Koerner, D. W., & Burgasser, A. J. 2003, AJ, 125, 3302

Golimowski, D. A., et al. 2004, AJ, 127, 3516

Gorlova, N. I., Meyer, M. R., Rieke, G. H., & Liebert, J. 2003, ApJ, 593, 1074

Guenther, E. W., & Wuchterl, G. 2003, A&A, 401, 677

Hambly, N. C., Davenhall, A. C., Irwin, M. J., & MacGillivray, H. T. 2001a, MNRAS 326, 1315

Hambly, N. C., Henry, T. J., Subasavage, J. P., Brown, M. A., & Jao, W.-C. 2004, AJ, 128, 473

Hambly, N. C., Irwin, M. J., & MacGillivray, H. T. 2001b, MNRAS 326, 1295

Hambly, N. C., MacGillivray, H. T., Read, M. A., et al. 2001c, MNRAS 326, 1279

Hawley, S. L. et al. 2002, AJ, 123, 3409

Henry, T. J., Jao, W.-C., Subasavage, J. P., Beaulieu, T. D., Ianna, P. A., Costa, E., & Méndez, R. A. 2006, AJ, 132, 2360

Joergens, V., & Müller, A. 2007, ApJ, 666, L113

Kasper, M., Biller, B. A., Burrows, A., Brandner, W., Budaj, J., & Close, L. M. 2007, A&A, 471, 655

Kendall, T. R., Delfosse, X., Martín, E. L., & Forveille, T. 2004, A&A, 416, L17

Kenyon, M. J., Jeffries, R. D., Naylor, T., Oliveira, J. M., & Maxted, P. F. L. 2005, MNRAS, 356, 89

Kirkpatrick, J. D. 2005, ARA&A, 43, 195

Kirkpatrick, J. D. Barman, T, S,, Burgasser, A. J., McGovern, M. R., McLean, I. S., Tinney, C. G., & Lowrance, P. J. 2006, ApJ, 639, 1120

Kirkpatrick, J. D., Beichman, C. A., & Skrutskie, M. F. 1997, ApJ, 476, 311

Kirkpatrick, J. D., Henry, T. J., & McCarthy, D. W., Jr. 1991, ApJS, 77, 417

Kirkpatrick, J. D., Reid, I. N., Liebert, J., Gizis, J. E., Burgasser, A. J., Monet, D. G., Dahn, C. C., Nelson, B., & Williams, R. J. 2000, AJ, 120, 447

Kirkpatrick, J. D., et al. 1999, ApJ, 519, 802

Knapp, G., et al. 2004, ApJ, 127, 3553

Kraus, A. L., White, R. J., & Hillenbrand, L. A. 2005, ApJ, 633, 452

Kurosawa, R., Harries, T. J., & Littlefair, S. P. 2006, MNRAS, 372, 1879

Leggett, S. K., Marley, M. S., Freedman, R., Saumon, D., Liu, M. C., Geballe, T. R., Golimowski, D. A., & Stephens, D. 2007, ApJ, 667, 537

Leggett, S. K., et al. 2000b, ApJ, 536, L35

Lépine, S., Rich, R. M., & Shara, M. M. 2003a, AJ, 125, 1598

Liebert, J., & Burgasser, A. J. 2007, ApJ, 655, 522

Liebert, J., & Gizis, J. E. 2006, PASP, 118, 659

Liebert, J., Kirkpatrick, J. D., Cruz, K. L, Reid, I. N., Burgasser, A. J., Tinney, C. G., & Gizis, J. E. 2003, AJ, 125, 343

Liu, M. C., & Leggett, S. K. 2005, ApJ, 634, 616

Liu, M. C., Leggett, S. K., & Chiu, K. 2007, ApJ, 660, 1507

Liu, M. C., Leggett, S. K., Golimowski, D. A., Chiu, K., Fan, X., Geballe, T. R., Schneider, D. P., & Brinkmann, J. 2006, ApJ, 647, 1393

Lodieu, N., Scholz, R.-D., McCaughrean, M. J., Ibata, R., Irwin, M., & Zinnecker, H. 2005, A&A, 440, 1061

Lodders, K. 1999, ApJ, 519, 793

Looper, D. L., Kirkpatrick, J. D., & Burgasser, A. J. 2007, AJ, 134, 1162

Looper, D. L., et al. 2008, ApJ, in preparation

Luhman, K. L., Joergens, V., Lada, C., Muzerolle, J., Pascucci, I., & White, R. 2007a, in Planets and Protostars V, eds. B. Reipurth, D. Jewitt and K. Keil (Univ. Arizona Press: Tucson), p. 443

Luhman, K. L., et al. 2007b, ApJ, 654, 570

Martín, E. L., Brandner, W., & Basri, G. 1999, Science, 283, 1718

Martín, E. L., Brandner, W., Bouy, H., Basri, G., Davis, J., Deshpande, R., Montgomery, M., & King, I. 2006, A&A, 456, 253

Martín, E. L., Delfosee, X., Basri, G., Goldman, B., Forveille, T., & Zapatero Osorio, M. R. 1999, AJ, 118, 2466

Maxted & Jeffries 2005, MNRAS, 326, L45

McCaughrean, M. J., Close, L. M., Scholz, R.-D., Lenzen, R., Biller, B., Brandner, W., Hartung, M., & Lodieu, N. 2004, A&A, 413, 1029

McElwain, M. W., & Burgasser, A. J. 2006, AJ, 132, 2074

McGovern, M. R., Kirkpatrick, J. D., McLean, I. S., Burgasser, A. J., Prato, L., & Lowrance, P. J. 2004, ApJ, 600, 1020

McLean, I. S., McGovern, M. R., Burgasser, A. J., Kirkpatrick, J. D., Prato, L., & Kim, S. 2003, ApJ, 596, 561

Mugrauer, M., Seifahrt, A., Neuhäuser, R., & Mazeh, T. 2006, MNRAS, 373, L31

Phan-Bao, N., Forveille, T., Martín, E. L., & Delfosse, X. 2006, ApJ, 645, L153

Pokorny, R. S., Jones, H. R. A., Hambly, N. C., & Pinfield, D. J. 2004, A&A, 421, 763

Potter, D., Martín, E. L., Cushing, M. C., Baudoz, P., Brandner, W., Guyon, O., & Neuhäuser, R. 2002, ApJ, 567, L133

Rayner, J. T., Toomey, D. W., Onaka, P. M., Denault, A. J., Stahlberger, W. E., Vacca, W. D., Cushing, M. C., & Wang, S. 2003, PASP, 155, 362

Reid, I. N., Burgasser, A. J., Cruz, K. L., Kirkpatrick, & J. D., Gizis 2001, AJ, 121, 1710

Reid, I. N., Gizis, J. E., Kirkpatrick, J. D., & Koerner, D. 2001b, AJ, 121, 489

Reid, I. N., Kirkpatrick, J. D., Gizis, J. E., Dahn, C. C., Monet, D. G., Williams, R. J., Liebert, J., & Burgasser, A. J. 2000, AJ, 119, 369

Reid, I. N., Kirkpatrick, J. D., Liebert, J., Gizis, J. E., Dahn, C. C., & Monet, D. G. 2002, AJ, 124, 519

Reid, I. N., Lewitus, E., Allen, P. R., Cruz, K. L., & Burgasser, A. J. 2006a, AJ, 132, 891

Reid, I. N., Lewitus, E., Cruz, K. L., & Burgasser, A. J. 2006b, ApJ, 639, 1114

Ruiz, M. T., & Takamiya, M. Y. 1995, AJ, 109, 2817

Scholz, R.-D., & Meusinger, H. 2002, MNRAS, 336, L49

Siegler, N., Close, L. M., Mamajek, E. E., & Freed, M. 2003, ApJ, 598, 1265

Siegler, N., Close, L. M., Cruz, K. L., Martín, E. L., & Reid, I. N. 2005, ApJ, 621, 1023

Siegler, N., Close, L. M., Burgasser, A. J., Cruz, K. L., Macintosh, B., Marios, C., & Barman, T. 2007, AJ, 133, 2320

Simons, D. A., & Tokunaga, A. T. 2002, PASP, 114, 169

Skrutskie, M. F., et al. 2006, AJ, 131, 1163

Stassun, K., Mathieu, R. D., Vaz, L. P. R., Valenti, J. A., & Gomez, Y. 2006, Nature, 440, 311

Strauss, M. A., et al. 1999, ApJ, 522, L61

Teegarden, B. J., et al. 2003, ApJ, 589, L51

Tinney, C. G., Burgasser, A. J., Kirkpatrick, J. D., & McElwain, M. W. 2005, AJ, 130, 2326

Tokunaga, A. T., & Kobayashi, N. 1999, AJ, 117, 1010

Tokunaga, A. T., Simons, D. A., & Vacca W. D. 2002, PASP, 114, 180

Tsvetanov, Z. I., et al. 2000, ApJ, 531, L61

Vacca, W. D., Cushing, M. C., & Rayner, J. T. 2003, PASP, 155, 389

van Biesbroeck, G. 1961, AJ, 66, 528

Vrba, F. J., et al. 2004, AJ, 127, 2948

Wallace, L., & Hinkle, K. 2001, ApJ, 559, 424

Wilson, J. C., Miller, N. A., Gizis, J. E., Skrutskie, M. F., Houck, J. R., Kirkpatrick, J. D., Burgasser, A. J., & Monet, D. G. 2003, in Brown Dwarfs (IAU Symp. 211), ed. E. Martín (San Francisco: ASP), p. 197

Wilson, J. C., et al. 2001b, AJ, 122, 1989

Zapatero Osorio, M. R., Lane, B. F., Pavlenko, Ya., Martín, E. L., Britton, M., & Kulkarni, S. R. 2004, ApJ, 615, 958

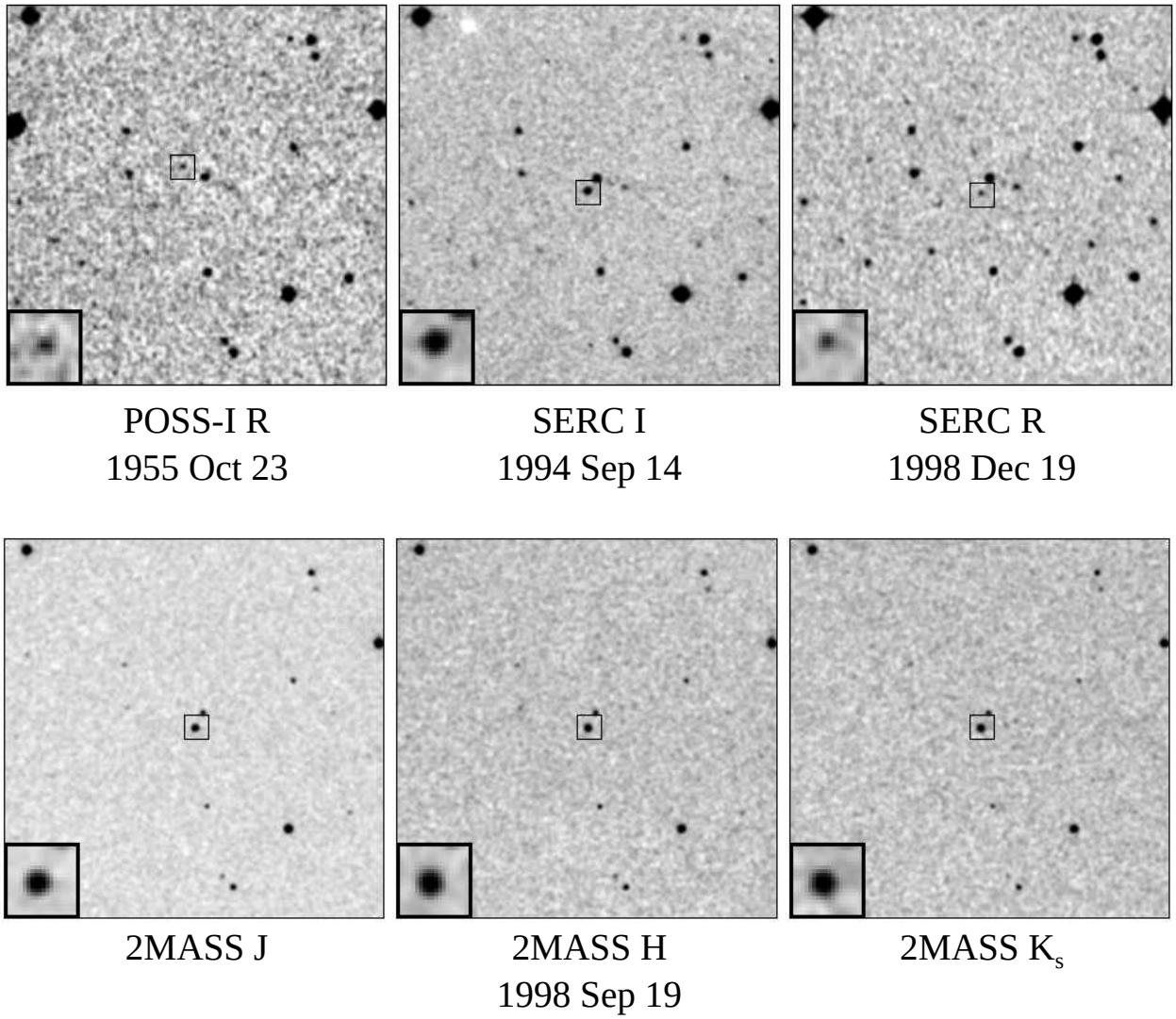

Fig. 1.— Field images of 2MASS J0320−0446 from ESO R (top left), SERC I_N (top middle) and SERC R (top right) photographic plates; and 2MASS JHK_s (bottom). All images are scaled to the same spatial resolution, are $5'$ on a side, and are oriented with north up and east to the left. Inset boxes $20''\times20''$ in size in each image indicate the position of the source after correcting for its motion ($\mu = 0\farcs562\pm0\farcs005$ yr^{-1} at position angle $\theta = 205\fdg9\pm0\fdg5$) and are expanded in the lower left corner of each image.

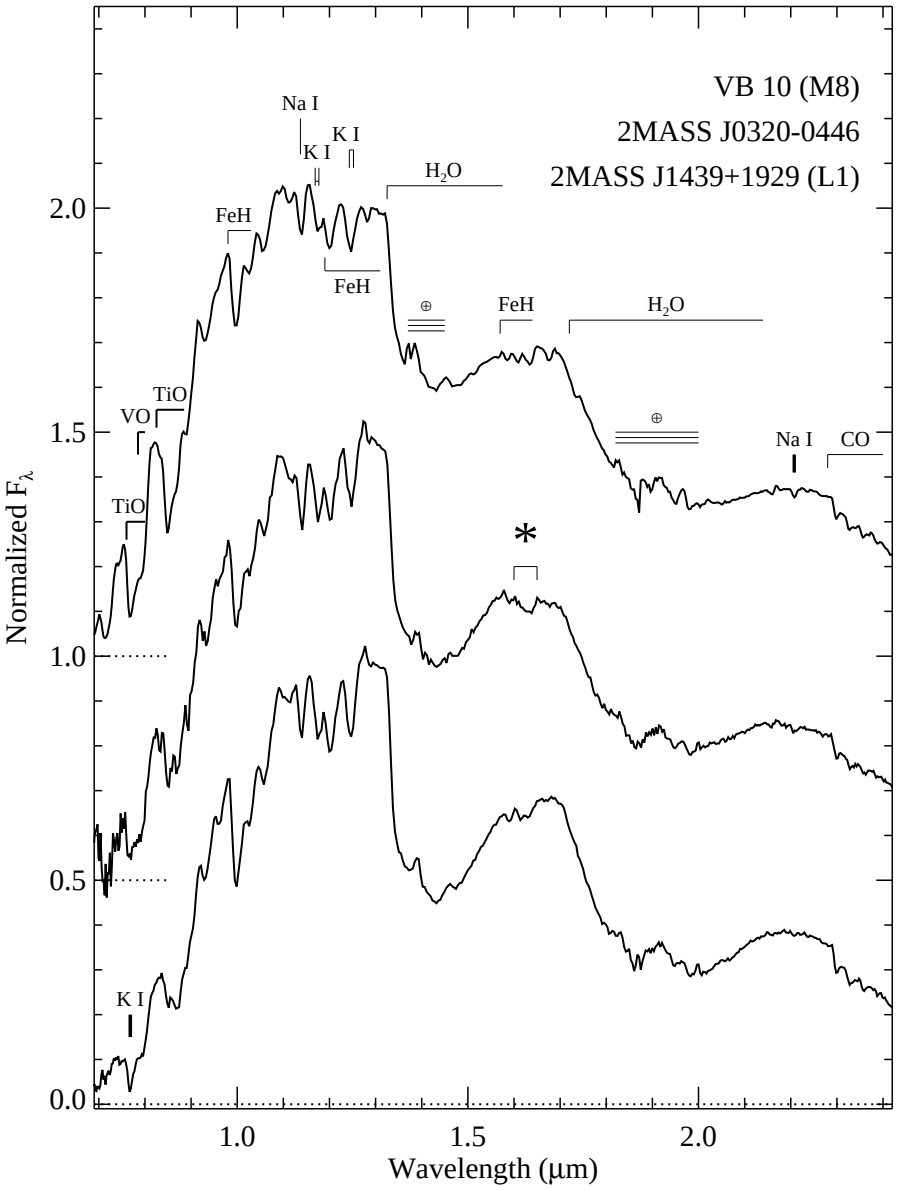

Fig. 2.— Reduced SpeX prism spectrum for 2MASS J0320−0446 (center) compared to equivalent data for VB 10 (M8) and 2MASS J1439+1929 (L1; see Table 3). Spectra are normalized at 1.25 μm and offset by constants (dotted lines). Prominent features resolved by these spectra are indicated. The peculiar 1.6 μm feature in the spectrum of 2MASS J0320−0446 discussed in the text is indicated by an asterisk.

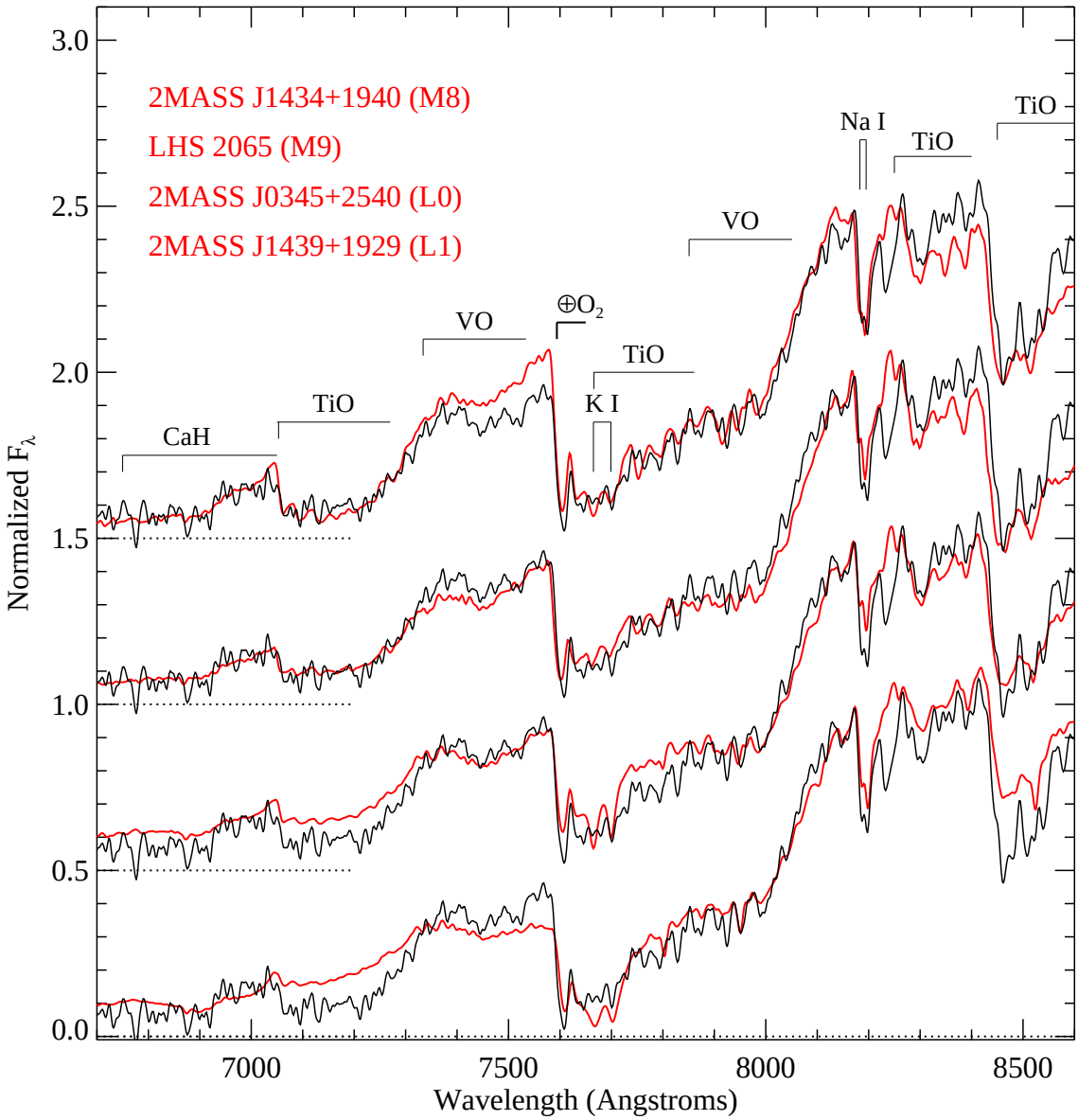

Fig. 3.— Optical spectrum of 2MASS J0320−0446 (black lines) from Cruz et al. (2003) overlain on equivalent data for (red lines, top to bottom) 2MASS J1434+1940 (M8), LHS 2065 (M9), 2MASS J0345+2540 (L0) and 2MASS J1439+1929 (L1; see Table 3). All spectra have been smoothed to a common resolution ($\lambda/\Delta\lambda = 800$), normalized at 8200 Å and offset by constants (dotted lines). Prominent spectral features are noted. Note that these data have not been corrected for telluric ($\oplus$) O_2 absorption.

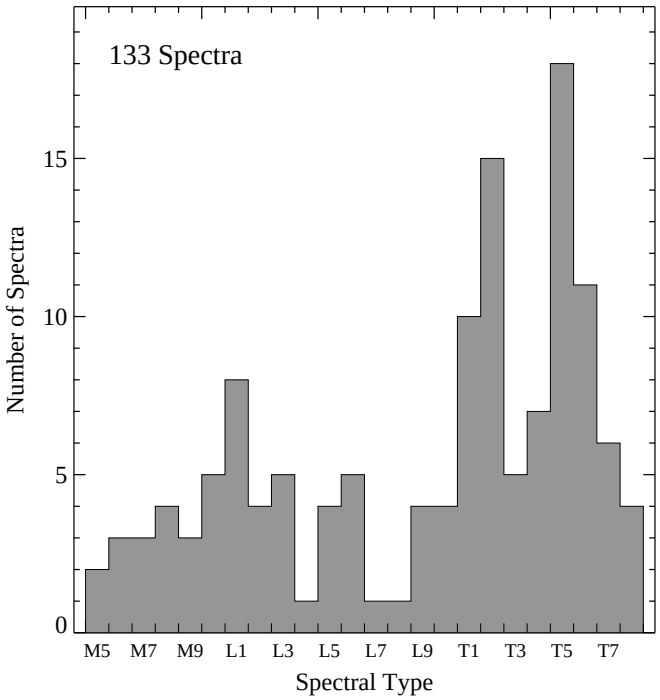

Fig. 4.— Distribution of spectral types in the SpeX prism spectral sample used to construct the binary templates. A total of 133 spectra of 126 sources were used.

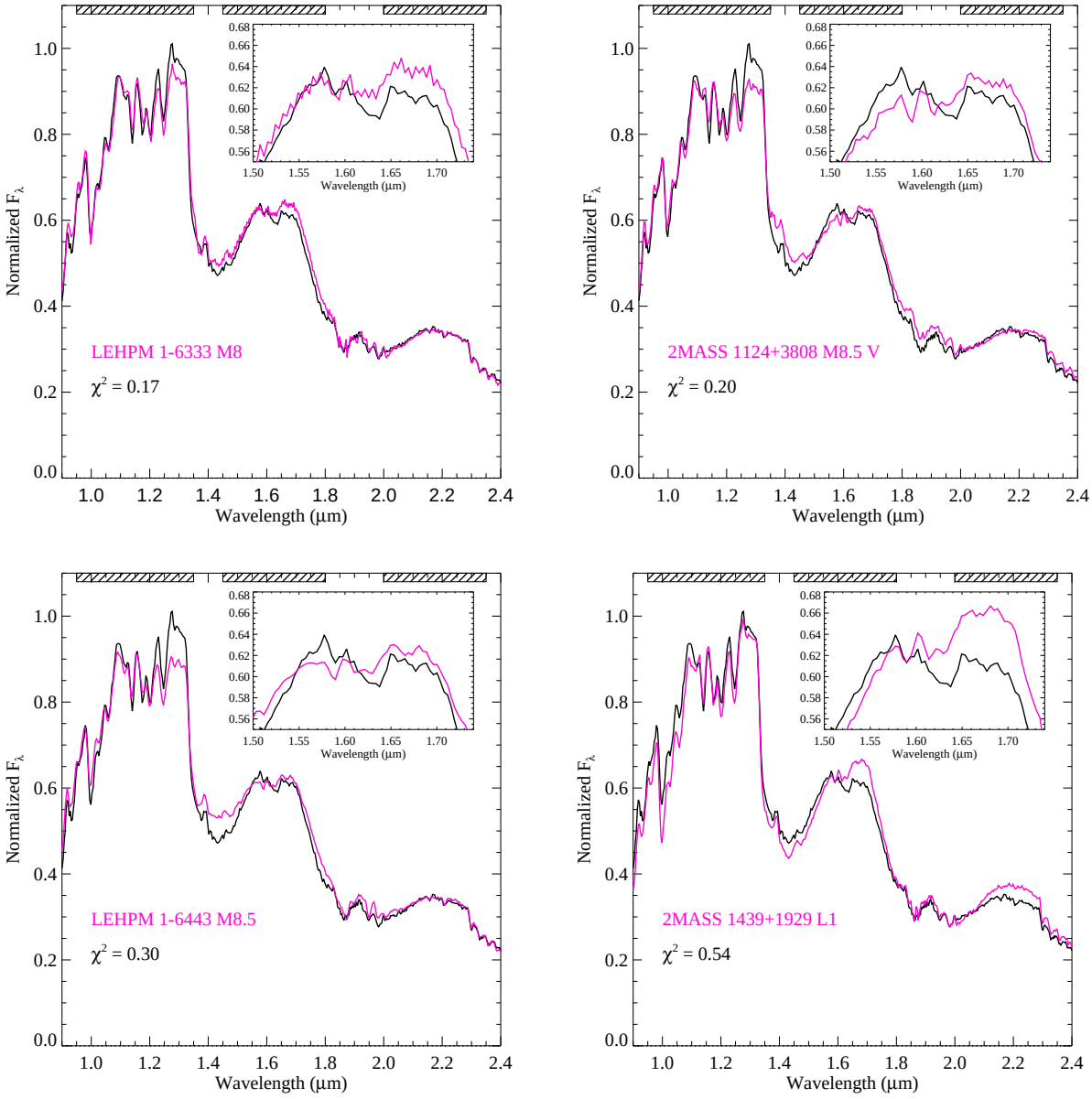

Fig. 5.— Best fit single spectral templates (purple lines) to the spectrum of 2MASS J0320−0446 (black lines): LEHPM 1-6333 (M8, $\chi^2 = 0.17$), 2MASS J1124+3808 (M8.5, $\chi^2 = 0.20$), LEHPM 1-6443 (M8.5, $\chi^2 = 0.30$) and 2MASS J1439+1929 (L1, $\chi^2 = 0.54$). All spectra are normalized in the 1.2–1.3 μm window, with the template further scaled to minimize their χ^2 deviations. The spectral bands used to calculate χ^2 are indicated at the top of each panel. Inset boxes show a close-up of the 1.5–1.75 μm region where the peculiar 1.6 μm feature present in the spectrum of 2MASS J0320−0446 is located.

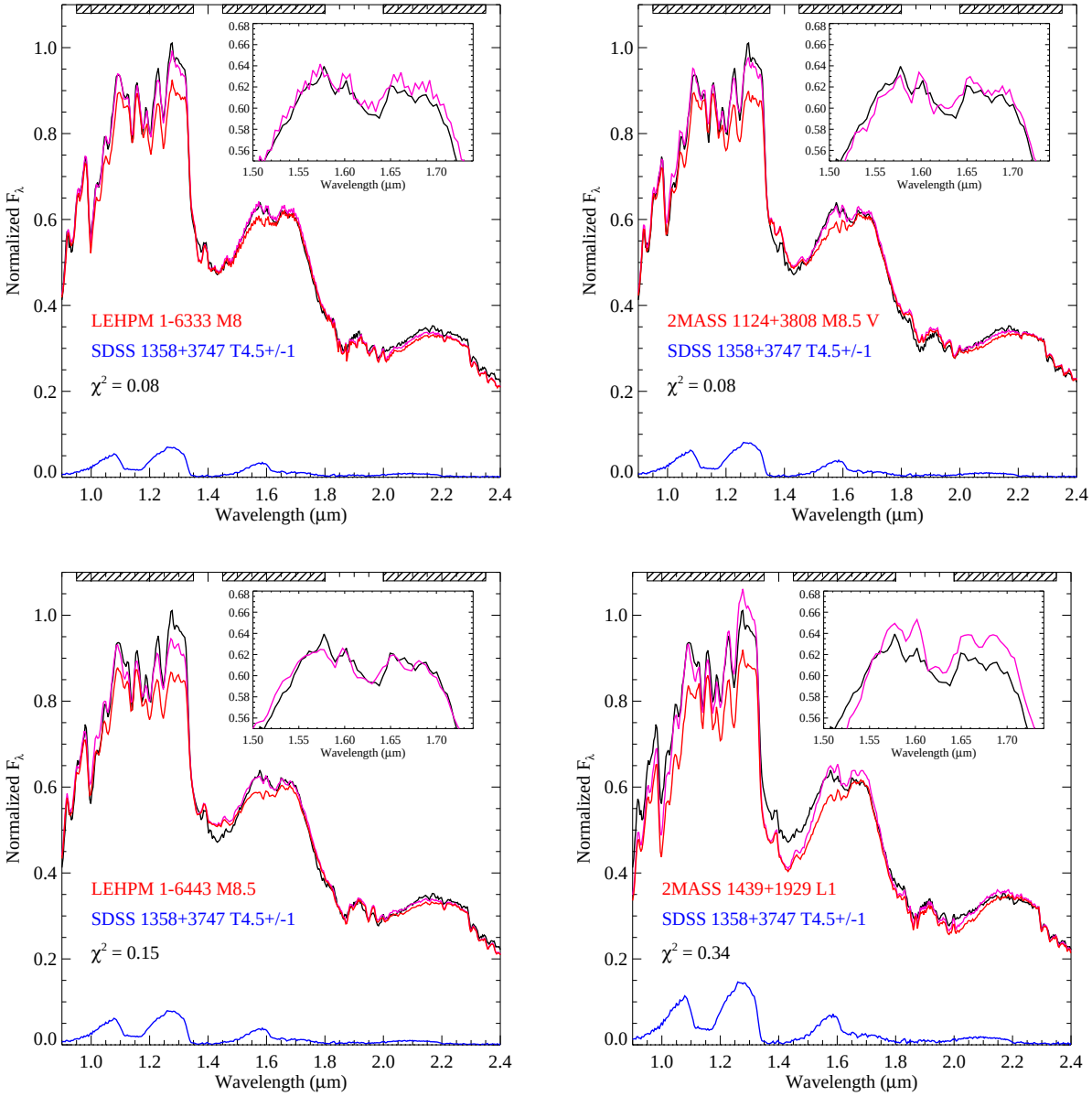

Fig. 6.— Best fit binary spectral templates (purple lines) to the spectrum of 2MASS J0320−0446 (black lines) constructed from the primaries shown in Figure 5 and using the "faint" M_K/spectral type relation of Liu et al. (2006). The primary (red lines) and secondary (blue lines) component spectra are scaled in accordance with their contribution to the binary templates. Inset boxes show a close-up of the 1.5–1.75 μm spectra of 2MASS J0320−0446 and best-fit binary templates.

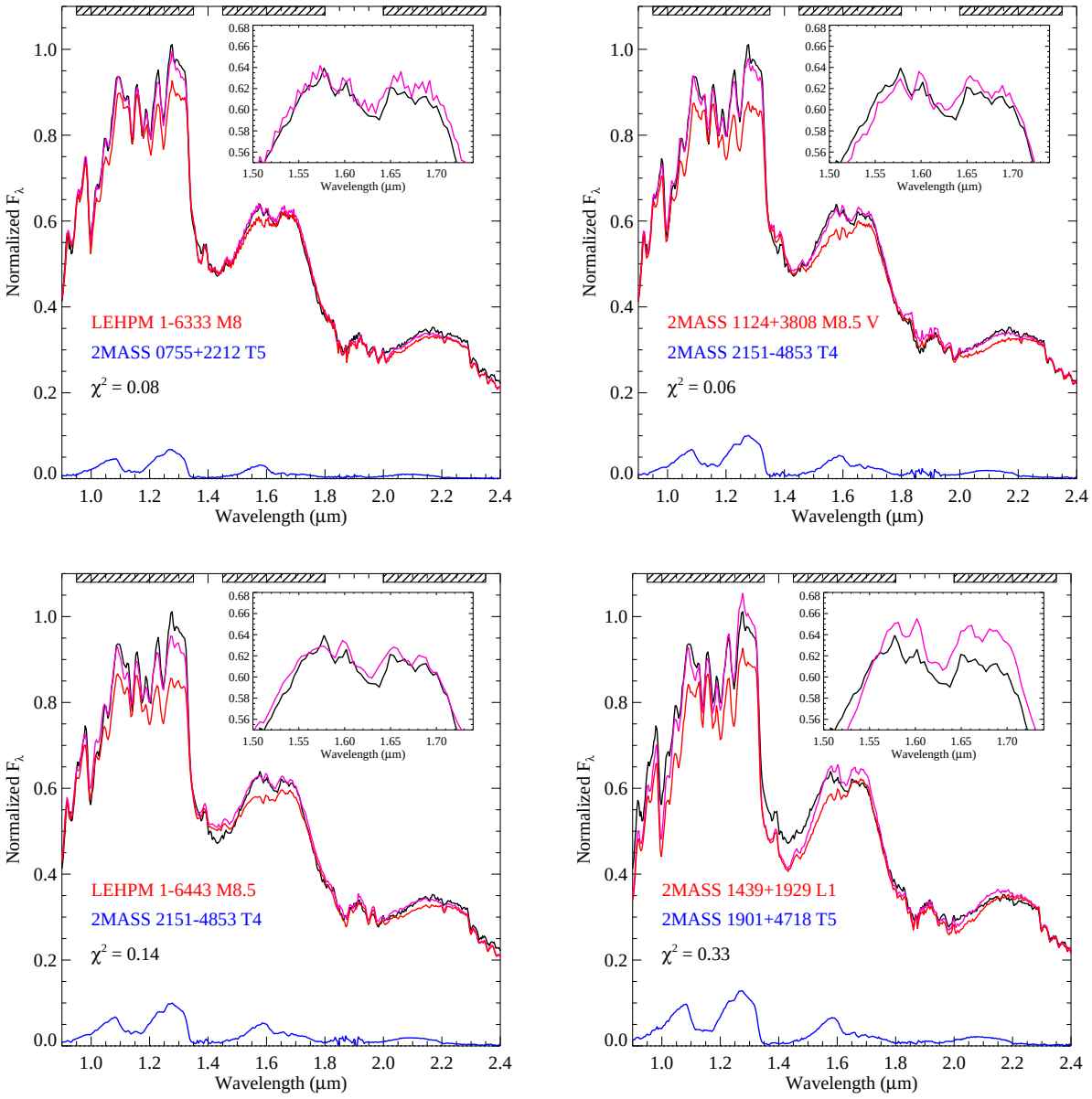

Fig. 7.— Same as Figure 7 but based on binary spectral templates constructed using the "bright" M_K/spectral type relation of Liu et al. (2006).

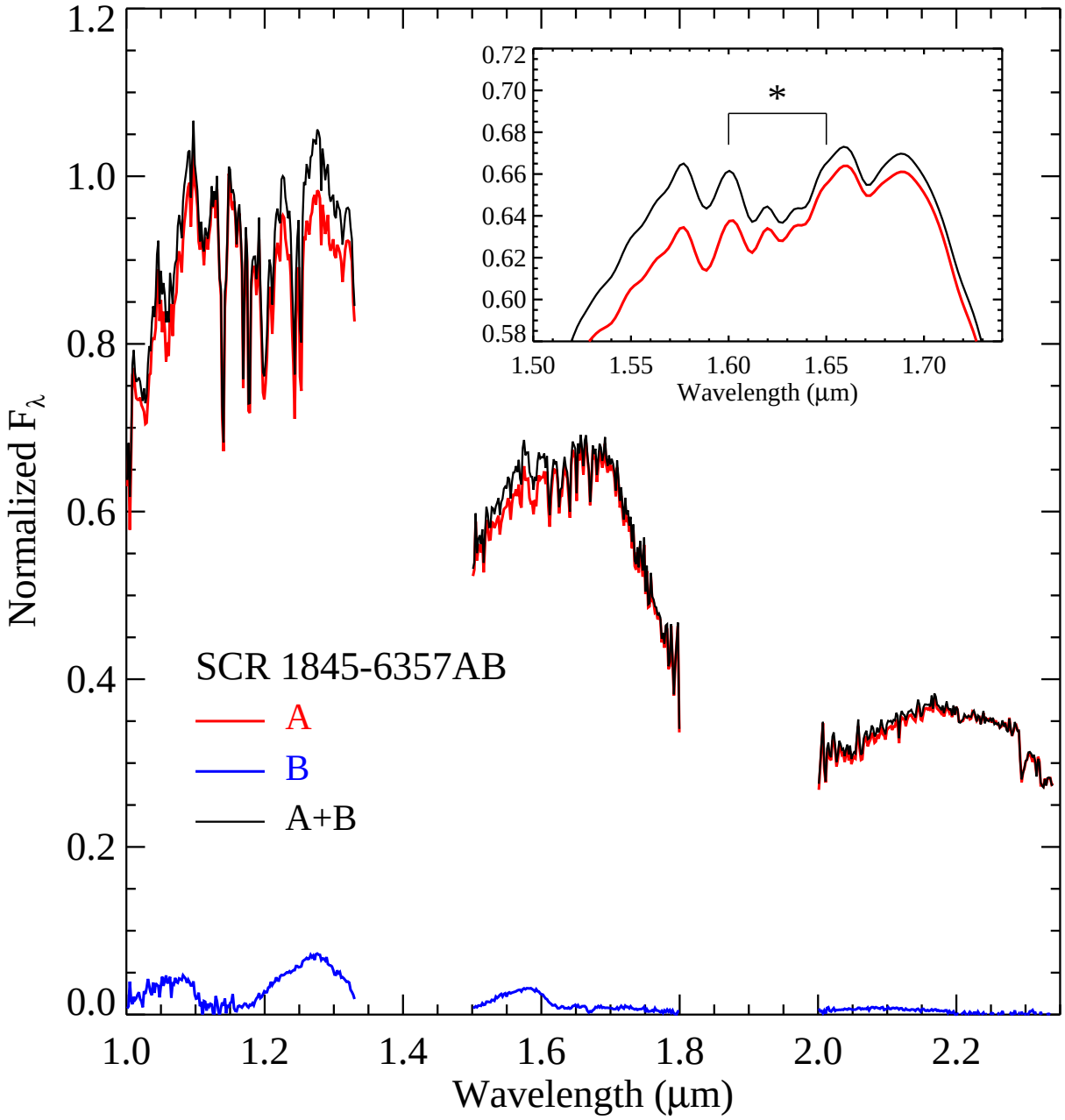

Fig. 8.— Component spectra of SCR 1845−6357AB from Kasper et al. (2007). The M8.5 primary (red lines) and T6 secondary (blue lines) spectra are scaled according to the relative H-band component photometry as reported by Kasper et al. The sum of the component spectra (black lines) shows a slight increase in both 1.25–1.35 μm and 1.55–1.6 μm flux. The inset box shows a close-up of the primary and composite spectra in the 1.5–1.75 μm region, where their spectral resolutions have been reduced to match that of the SpeX prism data. A weak 1.6 μm dip, similar to that seen in the spectrum of 2MASS J0320−0446, is also found to be present in the composite SCR 1845-6357 spectrum.

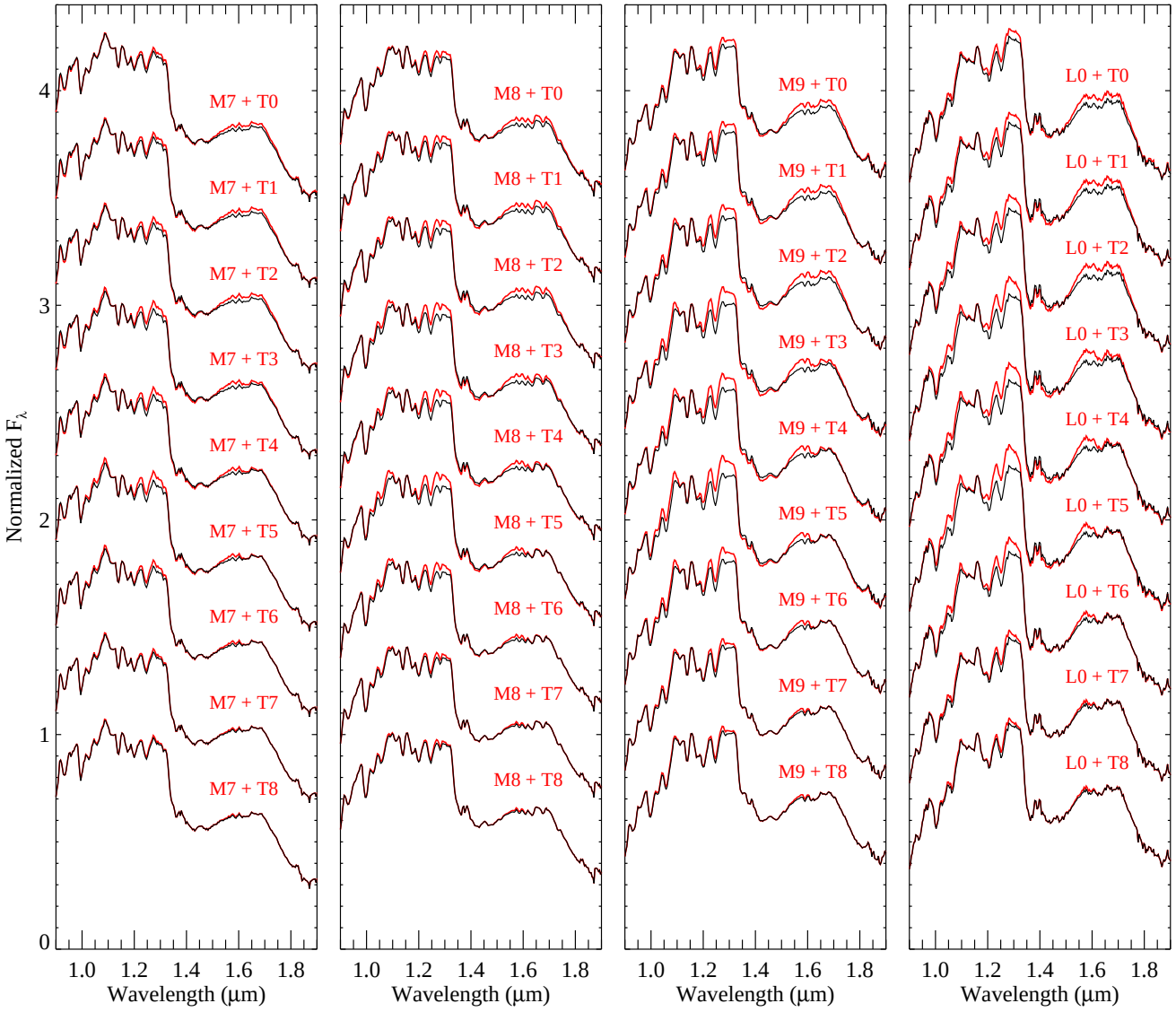

Fig. 9.— Simulated M7–L0 plus T dwarf binary spectra (red lines), based on the "bright" M_K/spectral type relation of Liu et al. (2006). The primaries shown (black lines) are VB 8 (M7), VB 10 (M8), LHS 2924 (M9) and 2MASS J0345+2540 (L0; see Table 3). The T dwarf secondaries are the standards defined in Burgasser et al. (2006a). Binary templates were constructed as described in § 3.3, and all spectra are normalized in the 1.12–1.17 μm region where the T dwarf companions contribute minimal flux.

Table 1. Astrometry for 2MASS J03202839−0446358.

α^{a}	δ^{a}	Epoch	Catalog
$03^h20^m29\overset{s}{.}09$	-04°46′13″.9	23 Oct 1955	POSS-I (R); SSS
$03^h20^m28\overset{s}{.}43$	-04°46′35″.3	14 Sep 1994	SERC (I_N); SSS
$03^h20^m28\overset{s}{.}39$	-04°46′35″.8	19 Sep 1998	2MASS
$03^h20^m28\overset{s}{.}38$	-04°46′35″.8	19 Dec 1998	SERC (R); SSS

[a]Equinox J2000 coordinates.

Table 2. Spectral Index Measurements for 2MASS J0320−0446.

Index	Feature	Value	SpT	Ref.
	Optical Indices			
VO2	0.79 μm VO	0.37	M8.5	1
TiO7	0.84 μm TiO	0.55	M7.5	1,2
PC3	Color ratio	2.04	M9	3,4
	Near Infrared Indices			
K1	K-band shape	0.15	L0.5	5,6
H_2O-A	1.4 μm H_2O	0.67	L2	6
H_2O-B	1.4 μm H_2O	0.81	L0.5	6
H_2O-1.5	1.4 μm H_2O	1.26	L0.5	4

References. — (1) Lépine, Rich, & Shara (2003a); (2) Hawley et al. (2002); (3) Martín et al. (1999); (4) Geballe et al. (2002); (5) Tokunaga & Kobayashi (1999); (6) Reid et al. (2001a)

Table 3. SpeX Spectral Templates.

Name	2MASS Designation[a]	Spectral Types		2MASS J	References[b]
		Optical	NIR		
SDSS J0000+2554	J00001354+2554180	···	T4.5	15.06±0.04	**1**;2
2MASS J0034+0523	J00345157+0523050	···	T6.5	15.54±0.05	**3**;1
2MASS J0036+1821	J00361617+1821104	L3.5	L4±1	12.47±0.03	**4**;2,5,6
HD 3651B	J0039191+211516	···	T7.5	16.16±0.03	**7**;8,9,10
2MASS J0050−3322	J00501994−3322402	···	T7	15.93±0.07	**11**;1,12
2MASS J0103+1935	J01033203+1935361	L6	···	16.29±0.08	**13**;6
2MASS J0117−3403	J01174748−3403258	L2:	···	15.18±0.04	**4**;14
SDSS J0119+2403	J01191207+2403317	···	T2	17.02±0.18	**15**
IPMS 0136+0933	J01365662+0933473	···	T2.5	13.46±0.03	**4**;16
2MASS J0144−0716	J01443536−0716142	L5	···	14.19±0.03	**4**;17
SDSS J0151+1244	J01514155+1244300	···	T1	16.57±0.13	**3**;1,18
2MASS J0205+1251	J02050344+1251422	L5	···	15.68±0.06	**19**;6
SDSS J0207+0000	J02074284+0000564	···	T4.5	16.80±0.16	**1**;18
2MASS J0208+2542	J02081833+2542533	L1	···	13.99±0.03	**4**;6
SIPS J0227−1624	J02271036−1624479	L1	···	13.57±0.02	**4**;20
2MASS J0228+2537	J02281101+2537380	L0:	L0	13.84±0.03	**4**;14,21
GJ 1048B	J02355993−2331205	L1	L1	···	**4**;22
2MASS J0241−1241	J02415367−1241069	L2:	···	15.61±0.07	**4**;14
2MASS J0243−2453	J02431371−2453298	···	T6	15.38±0.05	**3**;1,23
SDSS J0247−1631	J02474978−1631132	···	T2±1.5	17.19±0.18	**15**
SO 0253+1625	J02530084+1652532	M7	···	8.39±0.03	**4**;24,25
DENIS J0255−4700	J02550357−4700509	L8	L9	13.25±0.03	**1**;26,27
2MASS J0310+1648	J03105986+1648155	L8	L9	16.03±0.08	**28**;1,6
SDSS J0325+0425	J03255322+0425406	···	T5.5	16.25±0.14	**15**
2MASS J0328+2302	J03284265+2302051	L8	L9.5	16.69±0.14	**4**;2,6
LP 944−20	J03393521−3525440	M9	···	10.73±0.02	**4**
2MASS J0345+2540	J03454316+2540233	L0	L1±1	14.00±0.03	**29**;2,30,31
SDSS J0351+4810	J03510423+4810477	···	T1±1.5	16.47±0.13	**15**
2MASS J0407+1514	J04070885+1514565	···	T5	16.06±0.09	**3**;1
2MASS J0415−0935	J04151954−0935066	T8	T8	15.70±0.06	**3**;1,23,32
2MASS J0439−2353	J04390101−2353083	L6.5	···	14.41±0.03	**28**;14
2MASS J0510−4208	J05103520−4208140	···	T5	16.22±0.09	**33**
2MASS J0516−0445	J05160945−0445499	···	T5.5	15.98±0.08	**4**;1,34
2MASS J0559−1404	J05591914−1404488	T5	T4.5	13.80±0.02	**1**;32,35
2MASS J0602+4043	J06020638+4043588	···	T4.5	15.54±0.07	**33**

Table 3—Continued

Name	2MASS Designation[a]	Spectral Types		2MASS J	References[b]
		Optical	NIR		
LEHPM 2−461	J06590991−4746532	M6.5	M7	13.64±0.03	**4**;36,37
2MASS J0727+1710	J07271824+1710012	T8	T7	15.60±0.06	**11**;23,32
2MASS J0729−3954	J07290002−3954043	···	T8	15.92±0.08	**33**
2MASS J0755+2212	J07554795+2212169	T6	T5	15.73±0.06	**1**;23,32
SDSS J0758+3247	J07584037+3247245	···	T2	14.95±0.04	**4**;1,2
SSSPM 0829−1309	J08283419−1309198	L2	···	12.80±0.03	**38**;39,40
SDSS J0830+4828	J08300825+4828482	L8	L9±1	15.44±0.05	**4**;18,27
SDSS J0837−0000	J08371718−0000179	T0±2	T1	17.10±0.21	**33**;1,32,41
2MASS J0847−1532	J08472872−1532372	L2	···	13.51±0.03	**42**;14
SDSS J0858+3256	J08583467+3256275	···	T1	16.45±0.12	**15**
SDSS J0909+6525	J09090085+6525275	···	T1.5	16.03±0.09	**15**
2MASS J0939−2448	J09393548−2448279	···	T8	15.98±0.11	**1**;12
2MASS J0949−1545	J09490860−1545485	···	T2	16.15±0.12	**1**;12
2MASS J1007−4555	J10073369−4555147	···	T5	15.65±0.07	**33**
2MASS J1010−0406	J10101480−0406499	L6	···	15.51±0.06	**19**
HD 89744B	J10221489+4114266	L0	L (early)	14.90±0.04	**4**;43
SDSS J1039+3256	J10393137+3256263	···	T1	16.41±0.15	**15**
2MASS J1047+2124	J10475385+2124234	T7	T6.5	15.82±0.06	**4**;1,32,44
SDSS J1048+0111	J10484281+0111580	L1	L4	12.92±0.02	**4**;45,46
SDSS J1052+4422	J10521350+4422559	···	T0.5±1	15.96±0.10	**4**;15
Wolf 359	J10562886+0700527	M6	···	7.09±0.02	**4**
2MASS J1104+1959	J11040127+1959217	L4	···	14.38±0.03	**3**;14
2MASS J1106+2754	J11061197+2754225	···	T2.5	14.82±0.04	**33**
SDSS J1110+0116	J11101001+0116130	···	T5.5	16.34±0.12	**11**;1,18
2MASS J1114−2618	J11145133−2618235	···	T7.5	15.86±0.08	**11**;1,12
2MASS J1122−3512	J11220826−3512363	···	T2	15.02±0.04	**1**;12
2MASS J1124+3808	J11240487+3808054	M8.5	···	12.71±0.02	**3**;14
SDSS J1206+2813	J12060248+2813293	···	T3	16.54±0.11	**15**
SDSS J1207+0244	J12074717+0244249	L8	T0	15.58±0.07	**33**;1,45
2MASS J1209−1004	J12095613−1004008	···	T3	15.91±0.07	**3**;1,27
SDSS J1214+6316	J12144089+6316434	···	T3.5±1	16.59±0.12	**15**
2MASS J1217−0311	J12171110−0311131	T7	T7.5	15.86±0.06	**11**;1,32,44
2MASS J1221+0257	J12212770+0257198	L0	···	13.17±0.02	**4**;47
2MASS J1231+0847	J12314753+0847331	···	T5.5	15.57±0.07	**3**;1
2MASS J1237+6526	J12373919+6526148	T7	T6.5	16.05±0.09	**48**;1,32,44

Table 3—Continued

Name	2MASS Designation[a]	Spectral Types		2MASS J	References[b]
		Optical	NIR		
SDSS J1254−0122	J12545393−0122474	T2	T2	14.89±0.04	**3**;1,32,44
2MASS J1324+6358	J13243559+6358284	···	T2	15.60±0.07	**33**
SDSS J1346−0031	J13464634−0031501	T7	T6.5	16.00±0.10	**11**;1,32,49
SDSS J1358+3747	J13585269+3747137	···	T4.5±1	16.46±0.09	**15**
2MASS J1404−3159	J14044941−3159329	···	T2.5	15.60±0.06	**33**
LHS 2924	J14284323+3310391	M9	···	11.99±0.02	**29**
SDSS J1435+1129	J14355323+1129485	···	T2±1	17.14±0.23	**15**
2MASS J1439+1929	J14392836+1929149	L1	···	12.76±0.02	**3**;31
SDSS J1439+3042	J14394595+3042212	···	T2.5	17.22±0.23	**15**
Gliese 570D	J14571496−2121477	T7	T7.5	15.32±0.05	**3**;1,32,50
2MASS J1503+2525	J15031961+2525196	T6	T5	13.94±0.02	**3**;1,32,51
2MASS J1506+1321	J15065441+1321060	L3	···	13.37±0.02	**28**;52
2MASS J1507−1627	J15074769−1627386	L5	L5.5	12.83±0.03	**28**;2,5,6
SDSS J1511+0607	J15111466+0607431	···	T0±2	16.02±0.08	**15**
2MASS J1526+2043	J15261405+2043414	L7	···	15.59±0.06	**3**;6
2MASS J1546−3325	J15462718−3325111	···	T5.5	15.63±0.05	**4**;1,23
2MASS J1615+1340	J16150413+1340079	···	T6	16.35±0.09	**33**
SDSS J1624+0029	J16241436+0029158	···	T6	15.49±0.05	**11**;1,53
2MASS J1632+1904	J16322911+1904407	L8	L8	15.87±0.07	**28**;1,31
2MASS J1645−1319	J16452211−1319516	L1.5	···	12.45±0.03	**4**;54
VB 8	J16553529−0823401	M7	···	9.78±0.03	**4**
SDSS J1750+4222	J17502385+4222373	···	T2	16.47±0.10	**1**;2
SDSS J1750+1759	J17503293+1759042	···	T3.5	16.34±0.10	**3**;1,18
2MASS J1754+1649	J17545447+1649196	···	T5	15.81±0.07	**4**
SDSS J1758+4633	J17580545+4633099	···	T6.5	16.15±0.09	**11**;1,2
2MASS J1807+5015	J18071593+5015316	L1.5	L1	12.93±0.02	**4**;14,21
2MASS J1828−4849	J18283572−4849046	···	T5.5	15.18±0.06	**3**;1
2MASS J1901+4718	J19010601+4718136	···	T5	15.86±0.07	**3**;1
VB 10	J19165762+0509021	M8	···	9.91±0.03	**3**
2MASS J2002−0521	J20025073−0521524	L6	···	15.32±0.05	**4**;55
SDSS J2028+0052	J20282035+0052265	L3	···	14.30±0.04	**3**;45
LHS 3566	J20392378−2926335	M6	···	11.36±0.03	**3**
2MASS J2049−1944	J20491972−1944324	M7.5	···	12.85±0.02	**3**
SDSS J2052−1609	J20523515−1609308	···	T1±1	16.33±0.12	**4,15**
2MASS J2057−0252	J20575409−0252302	L1.5	L1.5	13.12±0.02	**3**;14,46

Table 3—Continued

Name	2MASS Designation[a]	Spectral Types		2MASS J	References[b]
		Optical	NIR		
2MASS J2107−0307	J21073169−0307337	L0	···	14.20±0.03	**3**;14
SDSS J2124+0100	J21241387+0059599	···	T5	16.03±0.07	**15**;1,2
2MASS J2132+1341	J21321145+1341584	L6	···	15.80±0.06	**4**;55
2MASS J2139+0220	J21392676+0220226	···	T1.5	15.26±0.05	**1**;56
HN Peg B	J21442847+1446077	···	T2.5	15.86±0.03	**9**
2MASS J2151−2441	J21512543−2441000	L3	···	15.75±0.08	**4**;55,57
2MASS J2151−4853	J21513839−4853542	···	T4	15.73±0.07	**4**;1,58
2MASS J2154+5942	J21543318+5942187	···	T6	15.66±0.07	**33**
2MASS J2212+1641	J22120345+1641093	M5	···	11.43±0.03	**3**
2MASS J2228−4310	J22282889−4310262	···	T6	15.66±0.07	**3**;1,34
2MASS J2234+2359	J22341394+2359559	M9.5	···	13.15±0.02	**3**
Gliese 866AB	J22383372−1517573	M5	···	6.55±0.02	**4**
SDSS J2249+0044	J22495345+0044046	L3	L5±1.5	16.59±0.13	**4**;2,18,45
2MASS J2254+3123	J22541892+3123498	···	T4	15.26±0.05	**3**;1,23
2MASS J2331−4718	J23312378−4718274	···	T5	15.66±0.07	**3**;1
2MASS J2339+1352	J23391025+1352284	···	T5	16.24±0.11	**1**;23
LEHPM 1−6333	J23515012−2537386	M8	M8	12.47±0.03	**4**;36,40,55
LEHPM 1−6443	J23540928−3316266	M8.5	M8	13.05±0.02	**4**;36,40
2MASS J2356−1553	J23565477−1553111	···	T5.5	15.82±0.06	**1**;23

[a]2MASS designations provide the sexigesimal Right Ascension and declination of each source at J2000 equinox: Jhhmmss[.]ss±ddmmss[.]s.

[b]Reference for spectral data in boldface type, followed by citations for source discovery and spectral classification, as listed at DwarfArchives.org.

References. — (1) Burgasser et al. (2006a); (2) Knapp et al. (2004); (3) Burgasser et al. (2004); (4) Burgasser et al., in preparation.; (5) Reid et al. (2000); (6) Kirkpatrick et al. (2000); (7) Burgasser (2007a); (8) Mugrauer et al. (2006); (9) Liu, Leggett, & Chiu (2007); (10) Luhman et al. (2007b); (11) Burgasser, Burrows & Kirkpatrick (2007); (12) Tinney et al. (2005); (13) Cruz et al. (2004); (14) Cruz et al. (2003); (15) Chiu et al. (2006); (16) Artigau et al. (2006); (17) Liebert et al. (2003); (18) Geballe et al. (2002); (19) Reid et al. (2006b); (20) Deacon, Hambly & Cooke (2005); (21) Wilson et al. (2003); (22) Gizis, Kirkpatrick, & Wilson (2001); (23) Burgasser et al. (2002); (24) Teegarden et al. (2003); (25) Henry et al. (2006); (26) Martín et al. (1999); (27) Kirkpatrick et al., in preparation; (28) Burgasser (2007b); (29) Burgasser &

McElwain (2006); (30) Kirkpatrick, Beichman & Skrutskie (1997); (31) Kirkpatrick et al. (1999); (32) Burgasser et al. (2003a); (33) Looper, Kirkpatrick & Burgasser (2007); (34) Burgasser, McElwain, & Kirkpatrick (2003); (35) Burgasser et al. (2000b); (36) Pokorny et al. (2004); (37) Ruiz & Takamiya (1995); (38) Burgasser et al. (2007a); (39) Scholz & Meusinger (2002); (40) Lodieu et al. (2005); (41) Leggett et al. (2000); (42) McElwain & Burgasser (2006); (43) Wilson et al. (2001); (44) Burgasser et al. (1999); (45) Hawley et al. (2002); (46) Kendall et al. (2004); (47) Reid et al., in preparation; (48) Liebert & Burgasser (2007); (49) Tsvetanov et al. (2000); (50) Burgasser et al. (2000a); (51) Burgasser et al. (2003b); (52) Gizis et al. (2000); (53) Strauss et al. (1999); (54) Gizis (2002); (55) Cruz et al. (2007); (56) Cruz et al., in preparation; (57) Liebert & Gizis (2006); (58) Ellis et al. (2005)

Table 4. Predicted Component Parameters for 2MASS J0320−0446.

Parameter	2MASS J0320−0446A	2MASS J0320−0446B	Difference
Spectral Type	M8.5±0.3	T5±0.9	···
J[a] (mag)	13.25±0.03	16.4±0.4	3.1±0.4
H[a] (mag)	12.61±0.03	16.4±0.5	3.8±0.5
K[a] (mag)	12.13±0.03	16.5±0.6	4.3±0.6
d (pc)	25±3	25±10	0±10
$\log_{10} L_{bol}/L_{\odot}$[b]	-3.48±0.10	-5.0±0.3	1.5±0.3
Mass ($M_{\odot}$) at 1 Gyr[c]	0.081	0.035	0.44[d]
Mass ($M_{\odot}$) at 5 Gyr[c]	0.086	0.068	0.79[d]
Mass ($M_{\odot}$) at 10 Gyr[c]	0.086	0.074	0.86[d]

[a]Synthetic magnitudes on the MKO system, based on 2MASS JHK_s photometry for the unresolved source and binary template fits using the "bright" M_K/spectral type relation of Liu et al. (2006).

[b]Based on the M_{bol}/spectral type relation of Burgasser (2007b).

[c]Based on evolutionary models from Burrows et al. (1997) and the estimated luminosities.

[d]Mass ratio M_2/M_1.